forum acusticum 2023

NONLINEAR BEHAVIOUR OF LOSSY ACOUSTIC BLACK HOLES

Olga Umnova[1*] **Daniel Brooke**[1] **Philippe Leclaire**[2] **Thomas Dupont**[3]
[1] University of Salford, Acoustic Research Centre, M5 4WT Salford, UK
[2] University of Burgundy, Drive - ISAT, 58000 Nevers, France
[3] ETS, University of Quebec, Montreal, Canada H3C 1K3

ABSTRACT

Sound absorption properties of acoustic black holes are studied for high pressure amplitudes. The absorbers consist of thin circular plates, each with a central perforation, separated by annular air cavities. Radius of the perforation of each plate depends on its position thus forming a central channel with a gradually decreasing radius. In our previous work, a linear equivalent fluid model accounting for the variations of the effective properties of air inside this channel was developed. However, the FEM simulations show that flow resistivity of the structure increases with the flow rate according to Forchheimer's law. This indicates that an extension of the model is necessary for the incident waves of high amplitude. In the current work, the measurements are performed for continuous high amplitude sound. A specially designed impedance tube is used for the experiments. The measurements and modelling show that the nonlinearity of acoustic black holes affects mostly the low frequencies. At higher frequencies, the absorption performance is weakly affected by the nonlinearity. This opens a possibility of using these structures as effective broadband absorbers of high amplitude sound.

Keywords: Acoustic Black Hole, sound attenuation, high amplitude sound, acoustic nonlinearity

1. INTRODUCTION

Starting from a pioneering work by Mironov and Pislyakov [1] the interest in acoustic absorbers with graded properties also known as Acoustic Black Holes (ABH) is steadily growing. ABHs typically consist of rigid annular thin plates separated by air cavities. Sound waves slowdown in the main channel of the ABH due to variations of the admittance of its walls. The latter is achieved by arranging the plates in such a way that their central perforation decreases with the distance from the surface of the absorber (see Figure 1).

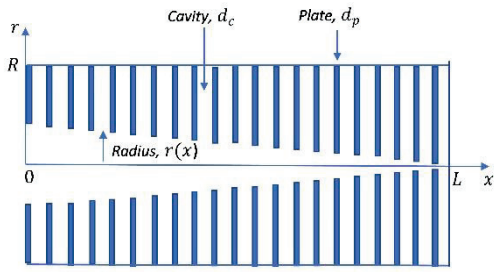

Figure 1. Schematic side view of the ABH absorber (Sample 1 from [2]). The actual sample contains 25 plates with central perforation radius gradually decreasing from 25 mm to 1 mm.

In lossy ABH [2] and similar "rainbow trapping" structures reported earlier [3] sound absorption in the broad range of frequencies is achieved due to thermoviscous losses in the main channel and in the narrow annular cavities between the plates. ABH absorbers are sturdy rigid structures, and this makes them suitable for the use in hostile environments for attenuation of high amplitude sound. For this, acoustical properties of ABHs for high amplitude sound must be studied. In the previous work [4] effective fluid model for "pancake" absorbers [5], [6] has been developed and extended to account for Forchheimer's nonlinearity. A deterioration of the absorption performance of the "pancake absorbers" has been demonstrated in experiments and confirmed by modelling. However, in some recent works e.g.

[*] ***Corresponding author***: o.umnova@salford.ac.uk.

[6]-[7] the microperforated panels and metamaterials were designed that show the improvement of the absorption performance at high SPL. In this work an extension of the equivalent fluid model for ABH [2] is performed to include nonlinear effects. The results of the nonlinear model are compared with the measurements for Sample 1 [2]. Also, a design is suggested which, according to the model, shows an improvement of absorption at high SPL compared to the linear results.

2. FLOW RESISTIVITY AND FORCHHEIMER'S NONLINEARITY PARAMETER

Static flow resistivity σ of the ABH absorber is calculated numerically using FEM. Laminar flow is modelled with the maximum Reynolds number much lower than 1000. The flow velocity V_f at the inlet varies to provide the dependence of flow resistivity on flow rate and approximate Forchheimer's parameter ξ

$$\sigma = \sigma_0(1 + \xi V_f) \tag{1}$$

The flow rate varies within the following range

$$10^{-6}\frac{m}{s} \le V_f \le 10^{-1}\frac{m}{s} \tag{2}$$

The limiting value of static flow resistivity σ_0 is found using linear interpolation as shown in Figure 2. Estimated static flow resistivity value is σ_0=12610 Pa s/m^2. Forchheimer's nonlinearity parameter value obtained from the simulations is ξ=7999 s/m. It should be noted that the value of flow resistivity σ_0 obtained numerically is higher than the one calculated for a channel with gradually decreasing cross section using equation (4.8.9) from [9]:

$$\sigma_0 = \frac{8\eta R^2}{L}\int_0^L \frac{dx}{r^4(x)} \tag{3}$$

where R is the radius of the tube, coinciding in our case with the outer radius of the sample and L is the length of the structure. If the radius of the channel decreases linearly with the distance x from the sample surface, so that

$$r(x) = r_{max} - \frac{r_{\max} - r_{min}}{L}x \tag{4}$$

then for the dimensions of Sample 1 equation (3) results in the following value for the flow resistivity of the channel

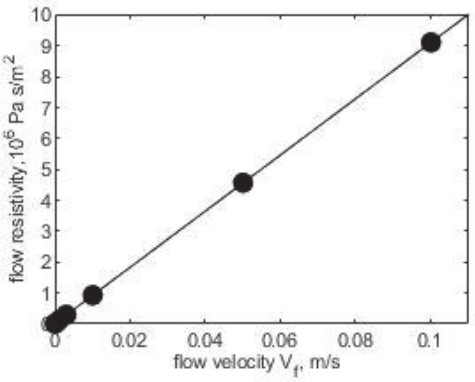

Figure 2. FEM results for flow resistivity dependence on flow velocity. Markers – FEM results, line – linear approximation y= $9.0779 \times 10^7 x + 12610$.

$$\sigma_0 = \frac{8\eta}{3}\frac{R^2}{r_{max}^2}\frac{r_{max}}{r_{min}^3}\frac{\left(1-\left(\frac{r_{min}}{r_{max}}\right)^2\right)}{\left(1-\frac{r_{min}}{r_{max}}\right)} = 4992\frac{Pa\ s}{m^2}. \tag{5}$$

However, flow resistivity calculated considering staircase variations of the channel radius (as shown in Figure 1) and assuming in-series arrangement of N=25 cylindrical channels with decreasing radii r_n results in the higher flow resistivity value

$$\sigma_0 = \frac{8\eta}{N}\sum_{n=1}^{N}\frac{R^2}{r_n^4} = 15585\frac{Pa\ s}{m^2}. \tag{6}$$

This is closer to the numerical result. In further calculations, the variations of the flow resistivity along the channel are considered for a staircase radius profile as was also done in [2], however numerically obtained value of Forchheimer's nonlinearity parameter which does not vary along the sample is used.

3. NONLINEAR GOVERNING EQUATIONS AND THEIR NUMERICAL SOLUTION

The frequency domain model used to calculate the dependence of absorption coefficient on incident pressure amplitude is based on the one developed in [3] for "pancake absorbers". The significant difference however is that the model for ABH accounts for the variations of the effective density and effective compressibility of the structure with the distance from its surface. As in [3], it is assumed that only

effective density is affected by acoustic nonlinearity of Forchheimer's type.
In this case, the equations for the normalized particle velocity (here all the notations are the same as those used for equations (37)-(38) in [2] and explained in Table 1)

$$V(X) = v(X)\frac{\phi_p(X)}{P_i\rho_0 c}$$

and normalized position dependent surface impedance of the ABH

$$Z(X) = \frac{1}{\rho_0 c}\frac{p(X)}{V(X)}$$

are the following

$$Z' = iq(\rho_m(X,V) - C_m(X)Z^2) \quad (7)$$

$$V' = iqC_m(X)VZ \quad (8)$$

where $q = kL$, $k = \frac{\omega}{c}$ is wavenumber in air.

$$\rho_m(X,V) = \frac{1}{\phi_p(X)}\left(1 + \frac{\sigma(X,V)}{-i\omega\rho_0}\sqrt{1 + \frac{-4i\omega\rho_0\eta}{\sigma^2(X,V)r^2(X)}}\right) \quad (9)$$

$$\sigma(X,V) = \frac{8\eta}{r^2(X)}\left(1 + \frac{\xi P_i}{\rho_0 c}|V|\right) \quad (10)$$

Equations (7)-(8) are solved with velocity boundary conditions at the surface of the sample

$$V(0) = \frac{2}{1 + Z(0)}, \quad (11)$$

which coincides with equation (43) from [4] if the normalisation by $\phi_p(X)$ is accounted for. The second condition is applied at the hard backing of the sample

$$V(1) = 0. \quad (12)$$

The absorption coefficient is calculated as

$$\alpha = 1 - \left|\frac{1 - Z(0)}{1 + Z(0)}\right|^2 \quad (13)$$

and depends on the incident pressure amplitude P_i due to dependence of flow resistivity on it as described by equation (10). Equations (7)-(8) with boundary conditions (11)-(12) are solved numerically using the method of iterations. In more detail, the method is described in [3].

X	Distance from the surface normalised to sample length L
v	Particle velocity in m/s
p	Acoustic pressure in Pa
P_i	Incident pressure amplitude in Pa
ϕ_p	Ratio of the channel surface area to that of the sample
ρ_m	Effective density of the material normalised by air density
C_m	Effective compressibility of the material normalised by compressibility of air
ρ_o	Density of air in kg/m^3
c	Sound speed in air in m/s
η	Air viscosity in $Pa \times s$

Table 1. List of notations.

4. RESULTS AND THEIR COMPARISONS WITH MEASUREMENTS

We start with absorption coefficient predictions of the linear model by setting ξ=0. In this case, equations (7)-(8) are reduced to a single equation (8) from reference [2] for the normalized position dependent admittance $\Gamma(X)=1/Z(X)$.
Predicted absorption coefficient dependence on frequency is shown in Figure 3. The first peak of the absorption coefficient (denoted as 1) is predicted at 228Hz and the second peak (denoted as 2) at 386 Hz. In the experiments the frequency of the first peak is 224 Hz and that of the second peak is 370 Hz. The nonlinear model was used to predict the dependence of the peak absorption coefficient values on incident pressure amplitude. The comparisons with the measurements using pure tones are shown in Figure 4a for the first peak and Figure 4b for the second peak.
It can be observed that the model correctly captures the main features of the absorption coefficient on incident pressure

amplitude P_i. The agreement with the data is very good for relatively low values of P_i. However, the agreement deteriorates for higher values.

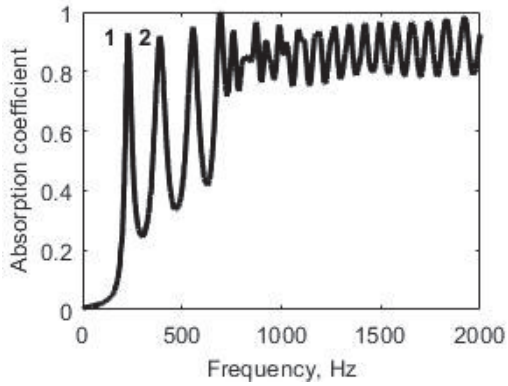

Figure 3. Absorption coefficient dependence on frequency, structure with 25 plates, linear model prediction.

This could be due to the nature of the model (iterations). Another reason for disagreement could be the use of constant value of Forchheimer's nonlinearity parameter. As the flow resistivity varies along the sample length (X dependence shown in equation (10)), the same could be expected for Forchheimer's parameter ξ. However, FEM simulations and the measurements could only give a value averaged over the sample. Inaccuracies in FEM model for flow resistivity which assumes laminar flow could contribute.

We now use the model to demonstrate the design which shows improvement of sound absorption at high amplitude of incident wave. For this we consider the structure with the plate closest to the backing is removed.

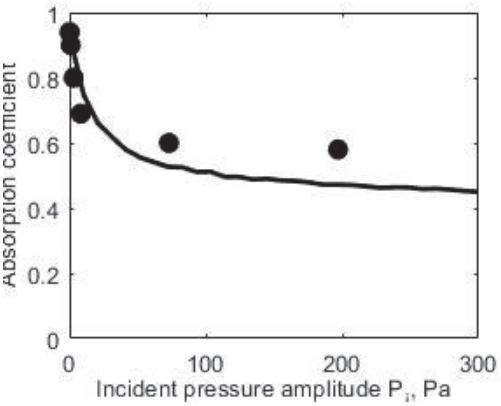

a

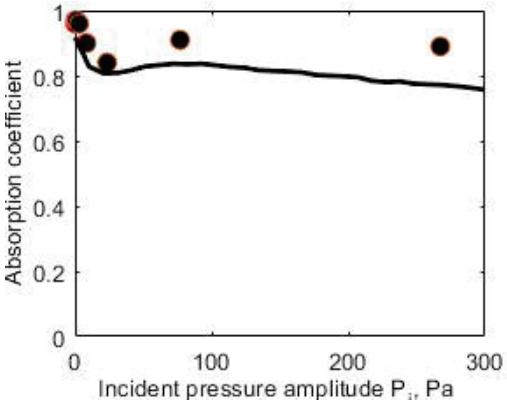

b

Figure 4. Absorption coefficient dependence on incident pressure amplitude. a – first peak, 228 Hz model (line), 224 Hz measurements (markers). b – second peak, 386 Hz model (line), 370 Hz measurements (markers).

The length of the structure is 96 mm and the minimum perforation radius is 2 mm. According to the model predictions, this small change in design leads to a significant deterioration of the absorption in the low frequency range. However, at higher amplitude of the incident sound a much-improved absorption is achieved. This is demonstrated in Figure 5.

5. CONCLUSIONS

The work presents the first results of modelling ABH absorption coefficient at high amplitudes of incident pressure wave. This model accounts for Forchheimer's nonlinearity responsible for the growth of flow resistivity of the main profiled channel with incident pressure amplitude. As the flow resistivity affects mainly

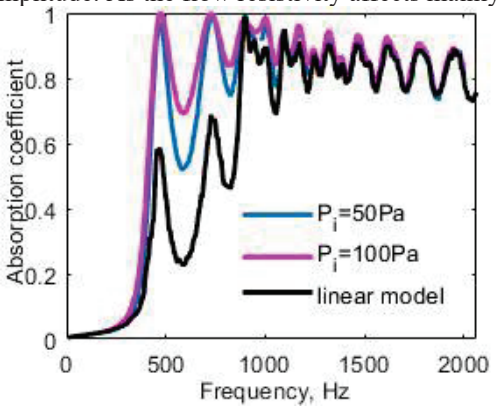

Figure 5. Absorption coefficient dependence on frequency for increasing incident pressure values, model predictions. Structure with 24 plates.

acoustical properties at low frequencies, a stronger dependence of the first absorption coefficient peak on incident pressure amplitude is predicted. This effect is also confirmed in measurements. For P_i=200 Pa the absorption coefficient decrease is 40% (50% model predictions) compared to its value for the low incident pressure amplitude. For the second peak the observed decrease is only 10% (20% model prediction). When the last plate is removed from the structure, the model predicts the improvement in absorption performance at high amplitudes, as illustrated in Figure 5. Future work will be focused on further experimental validations and on extension of the model to explain reflection data for high amplitude pulses. Particular attention will be given to the designs achieving nearly total absorption of high amplitude sound.

5. ACKNOWLEDGMENTS

Daniel Brooke has been supported by DSTL UK Anglo-French PhD scheme.

6. REFERENCES

[1] M.A Mironov, V.V. Pislyakov, One-dimensional acoustic waves in retarding structures with propagation velocity tending to zero. Acoust. Phys. 48, 347-352 (2002).

[2] O.Umnova, D.C. Brooke, P. Leclaire, T. Dupont, Multiple resonances in lossy acoustic black holes - theory and experiment. J. Sound Vib. 540, 117377 (2023).

[3] N. Jiménez, V. Romero-García, V. Pagneaux, J.-P.Groby, Rainbow-trapping absorbers: broadband, perfect and asymmetric sound absorption by subwavelength panels for transmission problems. Sci. Rep. 7, 13595 (2017).

[4] D.C.Brooke, O.Umnova, P.Leclaire, T. Dupont, Acoustic metamaterial for low frequency sound absorption in linear and nonlinear regimes. J. Sound Vib. 485, 115585 (2020).

[5] P. Leclaire, O. Umnova, T. Dupont, and R. Panneton, Acoustical properties of air-saturated porous material with periodically distributed dead-end pores. J. Acoust. Soc. Am. 137, 1772-1782 (2015).

[6] T. Dupont, P. Leclaire, R. Panneton, and O. Umnova, A microstructure material design for low frequency sound absorption. Appl. Acoust. 136, 86–93 (2018)

[7] Z. Laly, N. Atalla, S.-A. Meslioui, Acoustical modelling of micro-perforated panel at high sound pressure levels using equivalent fluid approach. J. Sound Vib. 427, 134 (2018).

[8] J. Zhu, H. Gao, S. Dai, Y. Qu, G. Meng, Multilayer structures for high-intensity sound energy absorption in low-frequency range. Int. J. Mech. Sci. 247, 108197 (2023).

[9] G.K. Batchelor, An introduction to fluid Dynamics, Cambridge University Press, 2002.